

An Isolation System for Racks on Board Vehicles

G. Di Massa, S. Pagano, S. Strano

Abstract— Trucks operating as mobile operation centers are equipped with cabinet-racks containing equipment sensitive to accelerations that must be preserved from mechanical shocks and vibrations. Therefore, racks on-board vehicles are often isolated to reduce the acceleration and the relative displacement amplitude to avoid impacts with surrounding bodies.

Racks inertial characteristics may change over time due to the replacement of the items; therefore, it is desirable to have an adjustable isolation system to guarantee the same isolation efficiency and the correct attitude of the isolated body.

In this paper, it is considered an isolation system constituted by air springs whose characteristics can be adjusted through the air pressure; it also includes wire rope stabilizers, to reduce pitch and roll oscillations, and magneto-rheological dampers to compensate the air spring low damping and to provide the ability to control the damping level in real time.

After the description of the isolation system, the results of the experimental characterization, conducted on each isolation component, are reported. These results were adopted to evaluate numerically the system isolation efficiency. Finally, the preliminary experimental tests conducted on a rack test rig are presented.

Index Terms— Air springs, MR dampers, shock isolation, vibration isolation, wire rope springs.

I. INTRODUCTION

TRUCKS working as mobile operation centers (i.e. mobile laboratories, remote broadcast television studios, military mobile tactical center, rescue command vehicles, etc.) are often equipped with many electronic devices (audio, video, networking, etc.) housed in rack-cabinets (Fig. 1) that are structures, characterized by standard sizes and standard fastening systems, in which the devices share the electric power unit and the cooling system. To accommodate many devices, two or more racks, can be connected to form a set of racks (Fig. 1b).

When racks are installed on board trucks, the devices may be subject to mechanical shocks and vibrations that may reduce their service life and their reliability. Mechanical excitations are due to internal sources (due to engine, power train, tire-wheel assembly, etc.) or to external sources deriving from road unevenness and, in general, from vehicle accelerations.

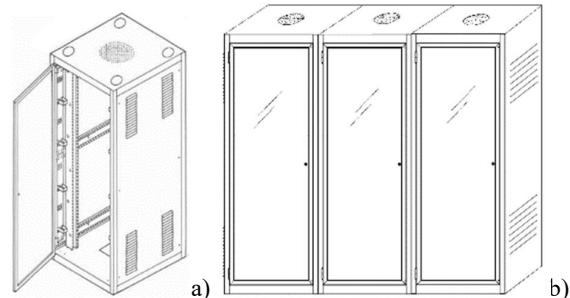


Fig. 1. a) Rack cabinet; b) set of three racks

The sprung mass of a truck is generally subject to $2.5 \div 3$ Hz ride vibrations; the acceleration is equal to $0.5 \div 1.0$ m/s^2 on paved road while it may reach 2 m/s^2 in case of unpaved roads and it can exceed 200 m/s^2 in presence of bumps or pits [1].

To preserve the devices from mechanical shocks and vibration coming from the truck chassis, the rack should be isolated. Racks installed in military trucks are isolated by means of wire rope isolators that are particularly suitable in absorbing mechanical shocks as they are capable of large deformations and thanks to an intrinsic damping due to the friction between the rope strands. The drawback of these springs is that they are designed for certain inertial characteristics of the rack and, if several devices are replaced with others having different mass, the isolation system loses its efficiency and the rack may assume a different static attitude.

The present paper examines the possibility of adopting a suspension system (Fig. 2), based on the adoption of air springs that, within certain limits, can tolerate the variation of the inertial characteristics of the isolated mass through the air pressure adjustment. The system requires an automatic system for the pressure regulation [2] and the introduction of dampers to compensate the air springs low damping. The proposed suspension system is therefore equipped with magneto-rheological dampers (MRDs) that allow the damping to be adjusted in real time. MRDs belong to the class of semi-active devices that are often preferred to the active ones since they require less energy and are not vulnerable to power or sensors failure. Indeed, semi-active devices are passive devices where the rheological properties (damping [3] or stiffness [4]) can be adjusted but they cannot input energy in the controlled system.

The first part of the paper describes the investigated suspension system and the results of several experimental tests carried out to characterize the isolation components; when adopting the test results, the isolation system efficiency is numerically investigated. In the final part, it is described the test rig that will be adopted to check the dynamic properties and to test the strategies to control the rack dynamic for the experimental investigation and the

Manuscript received July 14, 2019; revised August 29, 2019.

G. Di Massa is with the *Dipartimento di Ingegneria Industriale, Università degli Studi di Napoli Federico II*, 80125 ITALY, (e-mail: giandomenico.dimassa@unina.it)

S. Pagano is with the *Dipartimento di Ingegneria Industriale, Università degli Studi di Napoli Federico II*, 80125 ITALY, (e-mail: stefano.pagano@unina.it)

S. Strano is with the *Dipartimento di Ingegneria Industriale, Università degli Studi di Napoli Federico II*, 80125 ITALY, (e-mail: salvatore.strano@unina.it)

preliminary results obtained by exciting it by means of a mono-axial vibrating table.

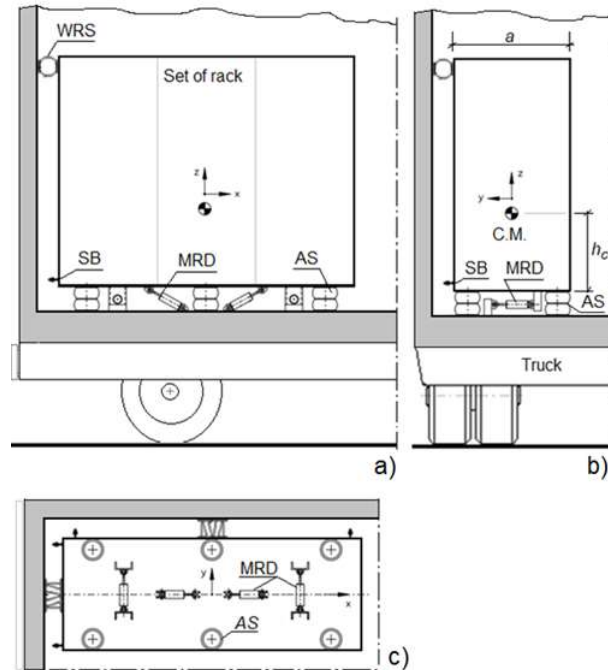


Fig. 2. Rack isolation scheme (AS: air springs; MRD: magnetorheological dampers; WRS: wire rope stabilizers; SB: stop bumpers)

II. THE ISOLATION SYSTEM COMPONENTS

As mentioned above, the isolation system consists of several elements; this section describes the component peculiarities and the criteria adopted to model them adequately.

A. Air springs

Air springs are capable of high strokes with a reduced initial height; they allow to realize vibrating systems having low natural frequencies, in comparison with other types of springs, with considerable advantage for the isolation efficiency. Its axial behavior has been widely studied, especially in the field of automotive and rail suspensions [5]. The air spring axial behavior may be defined by means of the thermodynamic *classical air spring model* [6] in which the air spring is modelled as a piston-cylinder system (Fig. 3) and the bellow stiffness contribution is neglected.

Therefore, by indicating with:

- p and A the internal pressure and the air spring effective transverse area;
- A_0 and p_0 the corresponding values at the equilibrium piston position z ,

the spring axial stiffness is defined by deriving the external vertical load with respect to the vertical displacement z :

$$k_z = \left. \frac{dP}{dz} \right|_0 = \frac{d}{dz} (pA)_0 = p_0 \frac{dA}{dz} + A_0 \frac{dp}{dz} \quad (1)$$

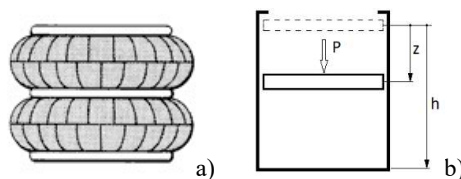


Fig. 3. Double convoluted air spring (a); air spring simplified model (b)

The model is based on the constancy of air mass and on the assumption that the air follows a polytropic process characterized by a polytropic index γ that is normally assumed equal to 1.38 for air springs. Differentiating the correspondent equation ($pV^\gamma = \text{const}$) and substituting the result in (1) it follows:

$$k_z = p_0 \frac{dA}{dz} - \frac{p_0 \gamma A_0}{V_0} \frac{dV}{dz} = p_0 \frac{dA}{dz} - \frac{p_0 \gamma}{(h-z)} \frac{dV}{dz} \quad (2)$$

being V the volume and dV/dz a negative quantity. Neglecting the effective area (A) variation, the vertical stiffness assumes the following expression (*simple air-spring model*):

$$k_z = - \frac{p_0 \gamma}{(h-z)} \left(A_0 \frac{d}{dz} (h-z) \right) = \frac{p_0 \gamma A_0}{(h-z)} = \frac{p_0 \gamma A_0^2}{V_0} \quad (3)$$

The axial stiffness depends on the displacement (z). However, it is possible to maintain the spring height constant, even for different loads, adjusting the air mass in the spring (compensated spring). In this case, the natural frequency of the suspended mass does not change with the weight since the axial stiffness will vary accordingly.

Regarding the air spring transverse characteristic, to date, to the best of the authors' knowledge, there isn't an analytical model to determine it. Several experimental investigations showed that the transverse stiffness mainly depends on the rubber element stiffness and on the axial load [7]; for this reason, the transverse stiffness is generally determined experimentally.

Air springs are characterized by a very low damping coefficient; therefore, they are often adopted in combination with dampers.

B. Magneto-rheological dampers

MRDs are constituted by a cylinder-piston system filled with magnetorheological fluid (Fig. 4). The piston head presents an orifice equipped with an electromagnet that induces a magnetic field in the fluid flowing through the orifice during the piston movement. By varying the current intensity circulating in the coil, damping can be continuously and rapidly adjusted with low power input [8].

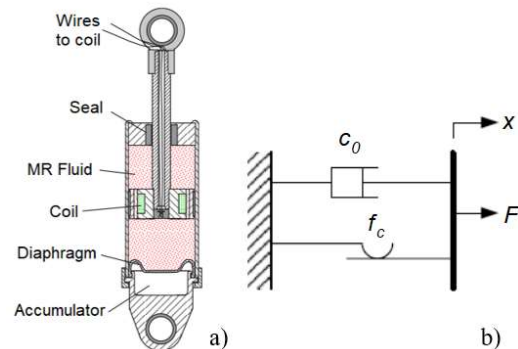


Fig. 4. MR damper (a) and the Bingham plastic model (b)

This type of damper has the advantage of combining the reliability of passive devices with the possibility of using

control methods to adapt the damping to the actual dynamic conditions of the system. [9].

The force exerted by an MRD may be modelled with the nonlinear Bingham model [10] that combines a viscous component in parallel with a Coulomb friction one (Fig. 4b):

$$F = c_0 \dot{x} + f_c \operatorname{sgn}(\dot{x}) + f_0 \quad (4)$$

being: \dot{x} , the excitation velocity; c_0 , the damping coefficient; f_c , the friction force related to the field-dependent yield stress; f_0 , is the offset force due to the presence of the (spring) accumulator (Fig. 4a), filled with compressed nitrogen, that is adopted to balance the volume changes due to the piston movements into the cylinder or to compensate the fluid thermal expansion.

C. Wire rope spring stabilizers

Since the height of the rack is greater than twice of the minor base dimension, the system tends to perform large roll and pitch oscillations with the risk of a collision with adjacent objects.

To contain roll and pitch oscillation, it is important that the body centre of mass is positioned toward the bottom of the base to minimize the *slenderness ratio*, defined as the ratio between (see Fig. 2 for reference) h_c , the centre of mass height and $a/2$ that is the minor base half-length: $s = h_c/(a/2)$. Its value may change over the time, due to the rack unit's replacement.

Roll and pitch amplitude oscillations may be limited by means of stabilizers, that are springs placed between the top of the rack and the walls of the truck body, mainly acting along the horizontal direction. In the present paper, stabilizers are constituted by helical wire rope springs (WRS) that are used for attenuating mechanical shocks as well as for absorbing wide-band vibrations.

Damping characteristics depend on several factors like cable diameter, number of strands, number of loops per isolator, lay angle of the strands, the overall dimensions of the isolator [11].

The insulation system has two stabilizers arranged on the rack top, at 90° to each other (Fig. 2); therefore, during roll rotation, one WRS works in tension-compression while the other one is shear deformed (Fig. 5); the opposite situation occurs for pitch motion.

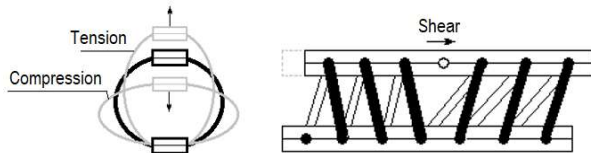


Fig. 5. WRS deformations

Experimental investigations have shown that these springs have a hardening behavior in tension and a softening behavior in compression. Several attempts were made to analytically define WRS stiffness and damping [12, 13]; in these attempts, the bending wire rope stiffness (EI) is considered constant though the elastic modulus (E) is load dependent and the cross-section moment of inertia (I) varies with the ring-coil deformation. In any case, they do not provide indications for the shear stiffness. Therefore, stabilizers characteristics

are generally deduced experimentally.

Due to friction forces among wire strands, wire rope can provide a significant level of dynamic damping that is typically 15% - 20% of critical damping. This level of damping makes wire rope springs attractive for applications that involve frequency sweeps through the resonance conditions and transients such as mechanical shock.

D. Stop bumpers

In case of large rack displacements, to avoid high accelerations due to the impact between rack and the walls of the rack cabin, rubber parabolic stop bumpers (Fig. 2) are adopted.

Other stop bumpers are placed next to the air springs to prevent excessive air springs axial deformation in case of insufficient air pressure; rack can rest on them even during the maintenance operations if air springs are not inflated.

Stop bumpers can absorb the energy in a progressive way; their effectiveness is due to the non-linear behaviour depending on the geometric shape and on the rubber material. The restoring force can be identified by means of experimental tests.

III. EXPERIMENTAL CHARACTERIZATION OF THE ISOLATION SYSTEM COMPONENTS

The characteristics of the isolation components were defined with reference to a set of three racks having external dimensions 1600x600x1780 mm; its mass can be considered equal to 1200 kg.

The isolation components were selected following the available indication in the component datasheets and were experimentally tested to detect the not available characteristics. This section describes the characterization tests and their results.

A. Air springs

Double-convoluted air springs, *Firestone mod.25*, were selected for the rack (fig.2). Their axial stiffness was determined on a press; the tests were performed by connecting an air spring to a 24 litres air reservoir by means of a pipe equipped with a valve. The results obtained for fully opened and fully closed valve are reported in Fig. 6a and Fig. 6b, respectively. Both tests were conducted considering the following initial condition: air pressure, 3 bar; axial load, 1400 N; spring height, 140 mm.

In the first case (Fig. 6a), the axial force varies with an almost linear trend with respect to the spring deformation; the axial stiffness can be considered constant with the axial deformation and equal to about 20 N/mm.

In the case of closed valve (Fig. 6b), the spring exhibits a hardening behaviour; the experimental axial stiffness, at the reference height (140 mm), is equal to: $k_z = 25.5$ N/mm. Then it increases up to about 100 N/mm for $h=80$ mm.

To identify the spring transverse characteristics, some experimental tests were carried out on a bi-axial press (Fig. 7), by loading the spring with a constant axial force and a periodic transverse one. To this end the air spring upper plate was axially loaded by means of a loading bar (Fig. 7); The spring lower plate was fixed on the horizontal slide of the

press, driven by a mechanical actuator, to perform a harmonic horizontal motion of assigned frequency and amplitude (± 5 mm). The test rig was equipped with a load cell and a displacement sensor to measure the horizontal force and the slide displacement.

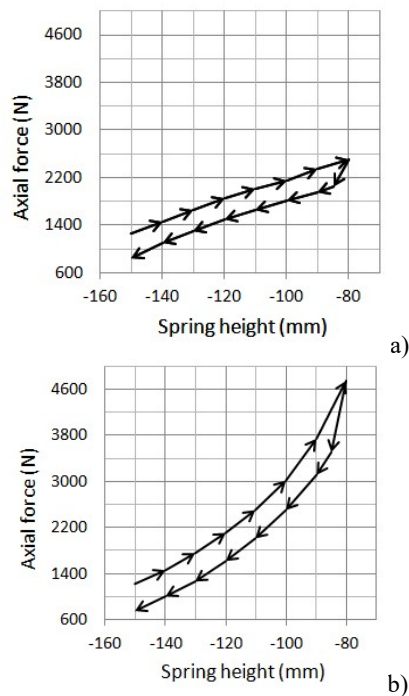


Fig. 6. Axial force vs spring height: a) fully opened valve; b) fully closed valve. Initial conditions: $F_z=1400$ N, $h=140$ mm, $p=3$ bar

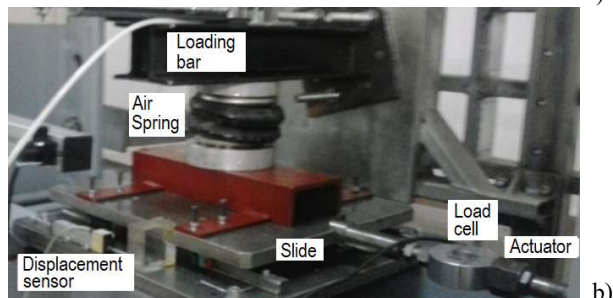
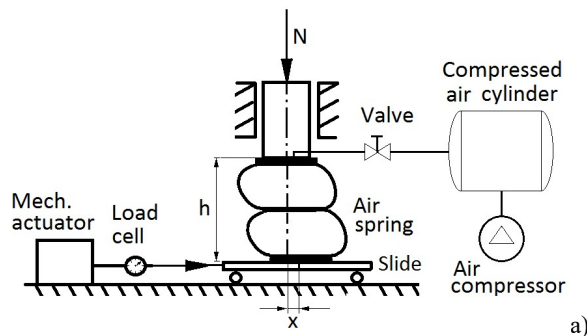


Fig. 7. Air spring under test: a) bi-axial press scheme; b) test equipment

Figs. 8 and 9 report the Force-Displacement diagrams obtained for a pressure of 2 bar at the spring height of 140 mm. The diagrams show that the horizontal restoring force linearly varies with the horizontal displacements; when the slide reverses, diagrams show a jump due to the change of sign of the friction force acting in the slide guides of the press. The slopes of the two parallel branches represents the

spring horizontal stiffness. The tests highlight that, decreasing the spring height, the transverse stiffness decreases until it results null (threshold of the static instability condition); beyond this value the stiffness is negative (static instability).

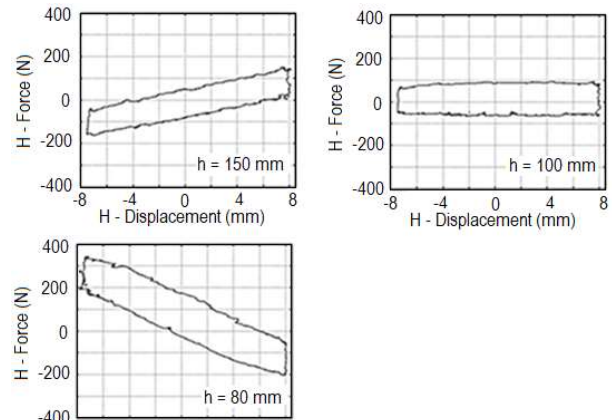


Fig. 8. F-D cycle with closed valve for $p = 2$ bar at 140 mm: a) $h = 150$ mm; b) $h = 100$ mm; c) $h = 80$ mm

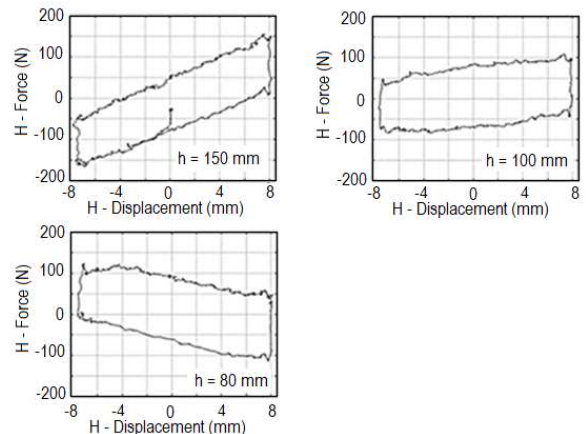


Fig. 9. F-D cycle with opened valve for $p = 2$ bar at 140 mm: a) $h = 150$ mm; b) $h = 100$ mm; c) $h = 80$ mm

The increasing pressure has a negative influence on the spring static stability. In fact, Force-Displacement diagrams show that the stiffness assumes null value for spring height of 100 mm, in the case of constant air mass (closed valve) while, at the same height, the spring is still stable in the case of variable air mass (opened valve).

The trends of the transverse stiffness versus the spring height are summarized in Fig. 10 that reports a comparison between the two operating conditions for three pressure values (2, 3 and 4 bar) assigned at the reference spring height (140 mm).

It can be noted that a bigger pressure value makes the spring unstable for a higher height, even if the horizontal stiffness is higher at the reference height. The experimental results show that at the reference height (140 mm), the spring is far enough away from static instability conditions.

B. Magneto-rheological dampers

Four MRDs (*Lord - mod. RD 8040-1*) were selected for the rack suspension (Fig.2); their main properties are provided by the manufacturer and are reported in Table I.

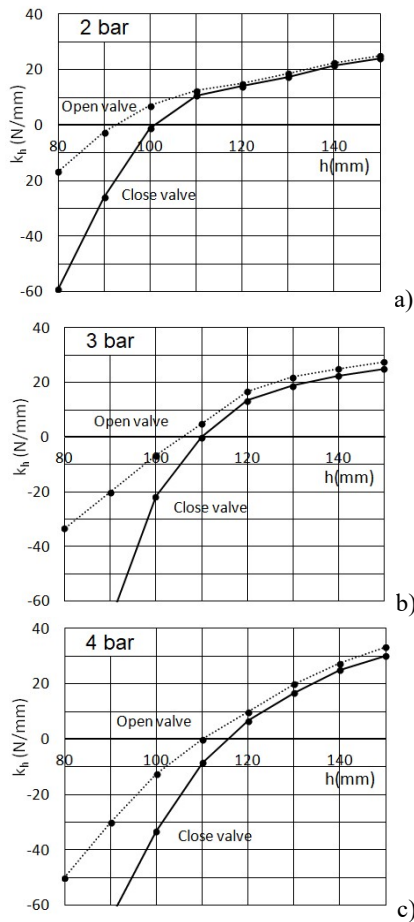


Fig. 10. Horizontal stiffness vs spring height with pressure at 140 mm: a) 2 bar; b) 3 bar; c) 4 bar

TABLE I
MR DAMPERS PROPERTIES (LORD, MOD. RD 8040-1)

Input current	2 A	Body diameter	42.1 mm
Input voltage	12 V _{DC}	Shaft diameter	10 mm
Resistance	5 Ω	Tensile strength	8896 N
Stroke	55 mm	Force (5 cm/s @ 1A)	>2447 N
Extended length	208 mm	Force (20 cm/s @ 0A)	<667 N

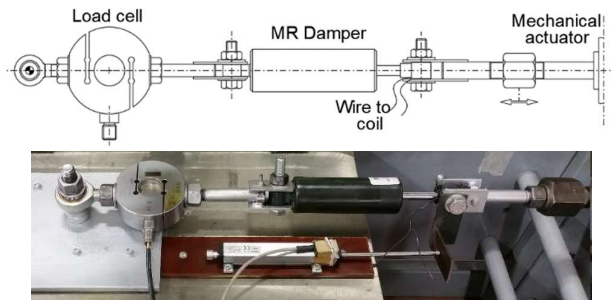


Fig.11. MRD under test: a) Scheme of the test equipment; b) test equipment

The damping force *versus velocity* was experimentally detected by adopting the test rig shown in Fig. 11. One extremity of the MR damper was connected to a load cell, fixed on the test rig frame; the other extremity is connected to a mechanical actuator that imposes a harmonic motion with

constant amplitude and adjustable frequency.

Force-Displacement and Force-Velocity diagrams were obtained for different current intensity circulating in the coil, adjustable in the range 0-2 A (Fig.12).

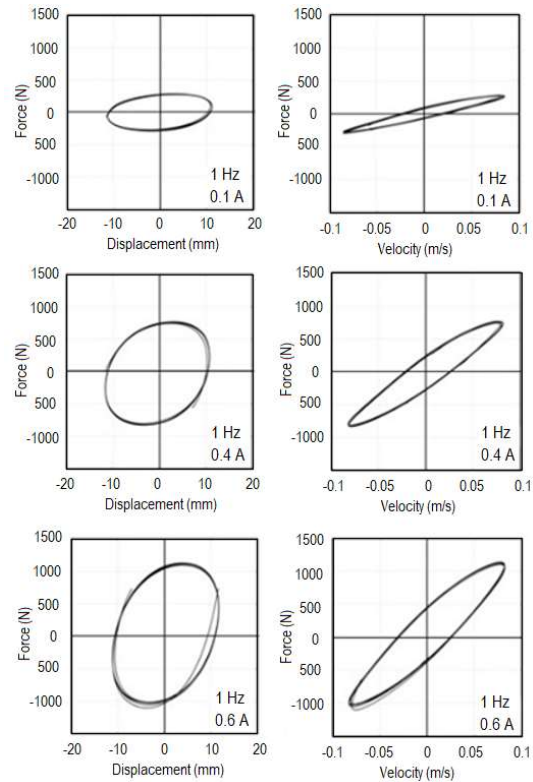


Fig. 12. Force-Displacement and Force-Velocity diagrams at 1 Hz, for different damper supply current

The energy loss in each cycle is related to the Force-Displacement loop area according to the following expression that gives the equivalent viscous coefficients [14]:

$$\sigma = A/(\pi\omega D^2) \tag{5}$$

being: A , the loop area; ω , the forcing circular frequency; D , the motion amplitude.

Repeating the tests for different values of the current supply intensity, the trend of the damping coefficient was identified for different forcing frequencies.

Diagrams in Fig. 13a report the damping coefficients vs MRD supply current intensity, for two forcing frequencies; the same data are reported even as damping coefficients vs forcing frequency (Fig. 13b). This last diagram shows that the damping decreases with the forcing frequency. This trend can be explained considering that the ferromagnetic particles chains in the MR fluid break if the yield stress is exceeded [15]; in the case of alternating motion, due to the inversion of the movement, the chains of particles break and reconstruct continuously; as the frequency increases, the reconstruction of the chains takes place with greater difficulty, involving a damping reduction; for this reason, all the curves tend asymptotically to that of the non-activated device (0 A). Fig. 13c reports the damper characteristic curves, i.e. the trend of the maximum damping force vs the maximum speed reached in the cycle.

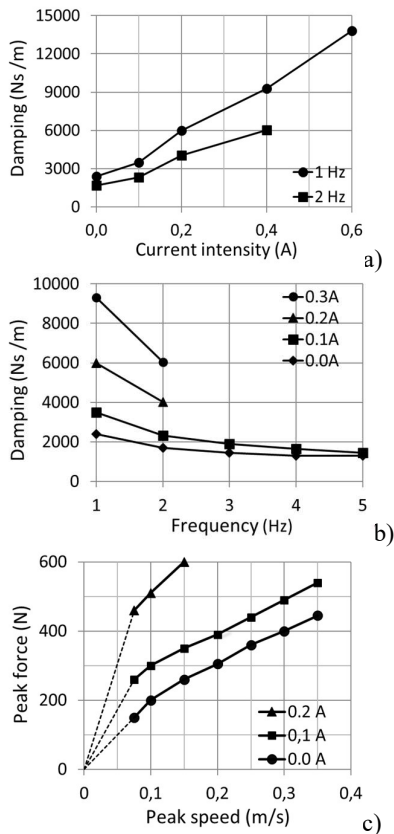


Fig. 13. MRD. a) damping vs current intensity; b) frequency; c) speed

The possibility of adjusting the damping will be adopted with the aim of reducing:

- displacement transmissibility in low frequency range (i.e. 0 – 1.5 Hz);
- acceleration transmissibility at higher frequencies (i.e. 1.5 – 30 Hz);
- displacement and acceleration overshoot and the consequent settling time due to bump excitations.

C. Wire rope spring stabilizers

The two stabilizers (Fig. 14, 24) are constituted by four coils helical wire rope springs (outside diameter, O.D. = 130 mm; cable diameter, $d = 6$ mm).

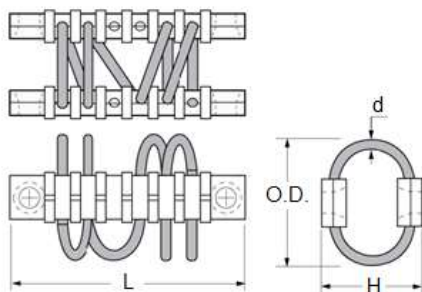


Fig. 14. Wire rope stabilizers

The spring characteristics were determined by means of static tests, by applying (separately) tension, compression and shear loads. The test results show that the spring exhibits a hardening behaviour in extension, a softening one in compression and a linear trend for shear load (Fig.15). The

softening behaviour in compression is due to the buckling of the helical loops.

Stabilizers exert a null restoring force when the rack is in the static equilibrium position; then, when the rack moves away from the truck walls, the restoring forces increase with a hardening trend assuming a high value at the end of the stroke, as the spring cables are almost completely extended. Instead, when the rack approaches the wall, the compressed stabilizers have a softening behaviour; to avoid the spring bottoming and the impact between racks and walls, several stop bumpers are adopted (Fig. 2).

The non-linear WRS dynamic behaviour is generally described by means hysteretic models [16]. Since these springs exert an appreciable action only in the case of significant deformations, in first approximation, a linear trend has been assumed and considering the test results, the following stiffness values can be considered: tension-compression stiffness: 5 N/mm; shear stiffness: 2 N/mm.

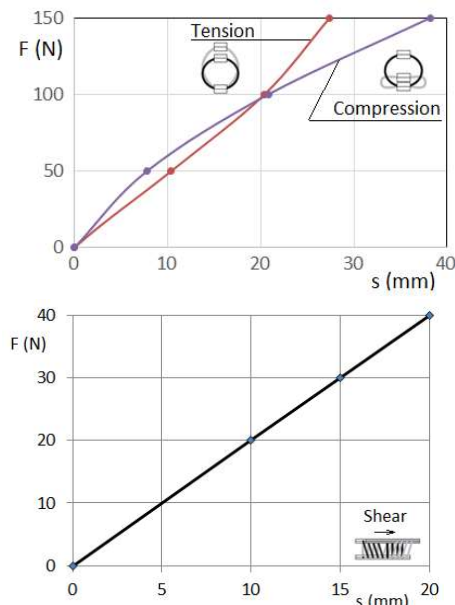


Fig. 15. a) Static WRS tension-compression characteristics; b) Static shear characteristic

D. Stop bumpers

In case of severe horizontal accelerations and wide displacements the rack energy is dissipated even by means of parabolic stop bumpers made of SBR (65 shore A). They exert their action if the maximum displacement is greater than 50 mm.

Two bumpers having different dimensions were adopted (Fig. 16): the smaller one is adopted to damp horizontal impact between rack and track walls while the bigger one is placed between rack and truck pavement (Fig.2).

The Force-Displacement diagrams were obtained by performing a quasi-static load test by means of a press. The devices were subjected to a slow loading/unloading cycle with a load rate of 0.1 mm/s. The correspondent diagrams show (Fig. 16) that they are very soft on the beginning of the contact with an evident hardening response.

It must be considered that elastomeric bumpers exhibit a larger stiffness if subjected to shock loading; the stiffness

increment depends on the load rate and it can be approximately considered 1.4 times the static stiffness.

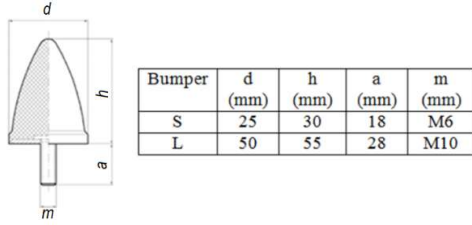


Fig. 16– Parabolic rubber stop bumpers

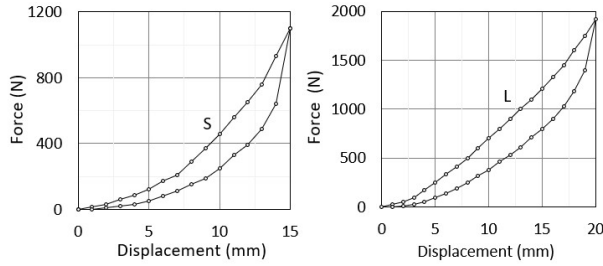


Fig. 17 – Force-Displacement trend for: a) bumper S; b) bumper L

IV. NUMERICAL SIMULATION

The rack can be modelled as a rigid body symmetric with respect to the two vertical reference planes (Fig. 2). The origin of the reference frame $Oxyz$ is placed in the geometric centre of the body; geometrical and inertial characteristics are reported in table II.

TABLE II
RACK GEOMETRICAL AND INERTIAL CHARACTERISTICS

Dimensions	$X = 1.60$ m; $Y = 0.60$ m; $Z = 1.78$ m
Mass	$m = 1200$ kg
CoG height (from the rack base)	$h_c = 0.52$ m
Moment of inertia	$I_{xx} = 587$ kg m ² ; $I_{yy} = 577$ kg m ² ; $I_{zz} = 360$ kg m ²

To reach the recommended air spring height of 140 mm, the air pressure has been set at 3 bar. In this condition the corresponding axial and shear linearized air spring stiffness are: $k_z = 25 \cdot 10^3$ N/m; $k_x = k_y = 22 \cdot 10^3$ N/m.

Damping and stiffness matrices (in the element reference system) are:

Air springs (N/m):

$$K_{air_spring} = \begin{bmatrix} 22 & 0 & 0 \\ 0 & 22 & 0 \\ 0 & 0 & 25 \end{bmatrix} \cdot 10^3 \quad (6)$$

Wire rope springs (N/m):

$$K_{wire_rope} = \begin{bmatrix} 2 & 0 & 0 \\ 0 & 2 & 0 \\ 0 & 0 & 5 \end{bmatrix} \cdot 10^3 \quad (7)$$

Wire rope damping (Ns/m):

$$C_{wire_rope} = \begin{bmatrix} 0.1 & 0 & 0 \\ 0 & 0.1 & 0 \\ 0 & 0 & 0.25 \end{bmatrix} \cdot 10^3 \quad (8)$$

MR (variable) damping (Ns/m):

$$C_{MR_dampers} = \begin{bmatrix} 0 & 0 & 0 \\ 0 & 0 & 0 \\ 0 & 0 & 2 \div 15 \end{bmatrix} \cdot 10^3 \quad (9)$$

In the hypothesis of small amplitude vibrations, a linear analysis is carried out below. Therefore, the presence of the stop bumpers, which provide their action only when the motion amplitude becomes large, is neglected.

Considering the position of each element in the rack reference frame, stiffness and damping matrices of the isolation system assume the following form:

$$[K] = \begin{bmatrix} 1.390 & & & -0.450 & -0.006 \\ & 1.390 & & 0.450 & -0.016 \\ & & 1.540 & 0.006 & 0.0160 \\ -0.450 & & 0.450 & 0.006 & 0.428 \\ -0.006 & -0.016 & & 0.016 & 0.763 & -0.008 & 0.451 \end{bmatrix} \cdot 10^5 \quad (10)$$

$[C_{max}] =$

$$= \begin{bmatrix} 1.520 & & & -0.289 & -0.003 \\ & 3.020 & & 1.204 & -0.008 \\ & & 1.520 & 0.003 & 0.008 \\ -0.289 & & 1.204 & 0.003 & 0.539 & 0.010 \\ -0.003 & -0.008 & & 0.008 & 0.106 & -0.004 & 0.757 \end{bmatrix} \cdot 10^4 \quad (11)$$

The equations of motion of the rack subjected to ground (truck floor) excitation are:

$$[M]\{\ddot{x}\} + [C]\{\dot{x}\} + [K]\{x\} = -[M]\{r\}a_G \quad (12)$$

being:

- $[M]$, the rack inertia matrix:

$$[M] = \begin{bmatrix} 1200 & & & & & & \\ & 1200 & & & & & \\ & & 587 & & & & \\ & & & 577 & & & \\ & & & & 360 & & \end{bmatrix} \quad (13)$$

- $\{x\} = \{x, y, z, \vartheta, \phi, \psi\}^T$, the vector containing displacements and rotations relative to the ground;
- a_G , the ground acceleration;
- $\{r\}$, the influence vector (depending on the ground excitation direction).

A. Stabilizers influence

A first approximate evaluation of the stabilizer influence is performed neglecting the MR damper actions and by comparing the normal modes frequencies and shape in absence and in presence of the stabilizers.

Neglecting the presence of the two WRSs, the isolation system is symmetrical with respect to the reference planes xz and yz . Indicating with f_j and $\{u\}$ the normal modes frequencies and mode shapes, obtained by solving the

eigenvalues problem, the modes participating factors matrix [L], whose rows represent the normal modes, can be evaluated:

$$[L] = \frac{\{u\}^T[M]}{\{u\}^T[M]\{u\}}$$

$$[L] = \begin{bmatrix} x & y & z & \vartheta & \varphi & \psi \\ 0 & -18.86 & 0 & 20.32 & 0 & 0 \\ 24.04 & 0 & 0 & 0 & 17.02 & 0 \\ 0 & 0 & 0 & 0 & 0 & 18.97 \\ 0 & 0 & -34.64 & 0 & 0 & 0 \\ 0 & 29.06 & 0 & 13.19 & 0 & 0 \\ 24.55 & 0 & 0 & 0 & -16.95 & 0 \end{bmatrix} \quad (14)$$

Due to the suspension system symmetry, z (bounce) and ψ (yaw) modes are uncoupled (rows 3 and 4 in the matrix) while, x is coupled with φ pitch rotation (rows 2 and 6) as well as y is coupled with ϑ roll rotation (rows 1 and 5). Mode shapes are reported in Fig 18a; next to each mode shape, the mode frequency and the mode damping factor (in brackets) are reported in the figure.

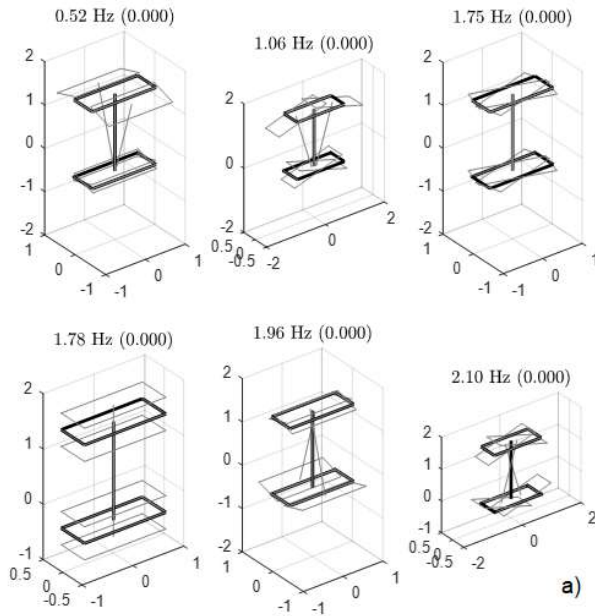


Fig. 18a. Modal shape for air springs height of 140 mm, without stabilizers, null damping.

The presence of the wire-rope stabilizers makes the system asymmetric; therefore, the vibration modes are (weakly) coupled, as shown by the mode shapes (Fig. 18b) and by the correspondent elements in the participating factor matrix:

$$[L] = \begin{bmatrix} x & y & z & \vartheta & \varphi & \psi \\ 0.07 & 19.39 & 0.22 & -20.03 & 0.05 & 1.09 \\ -26.23 & 0.09 & 0.734 & -0.09 & -15.67 & -0.60 \\ -1.14 & -1.67 & -0.07 & 0.88 & -0.26 & 18.93 \\ -1.20 & 0.61 & -34.61 & 0.10 & 0.19 & -0.04 \\ 0 & -28.65 & -0.58 & -13.60 & 0.01 & -0.37 \\ 22.57 & 0 & -1 & 0 & -18.21 & 0.25 \end{bmatrix} \quad (15)$$

Stabilizers have the effect of substantially modifying only the first two natural frequency (roll, pitch), as highlighted in

Fig. 19. Modes shapes allow to evaluate which of them can be truly damped by MR-dampers, due to their arrangement and to the position of the mode oscillating axis. For example, dampers placed under the rack and acting in yz plane cannot efficiently influence the first vibrating mode, as they are too close to the rotation axis. Similarly, damper placed under the rack and acting in xz plane, cannot efficiently damp the second vibrating mode; however, these two modes are damped by the stabilizers dissipative action.

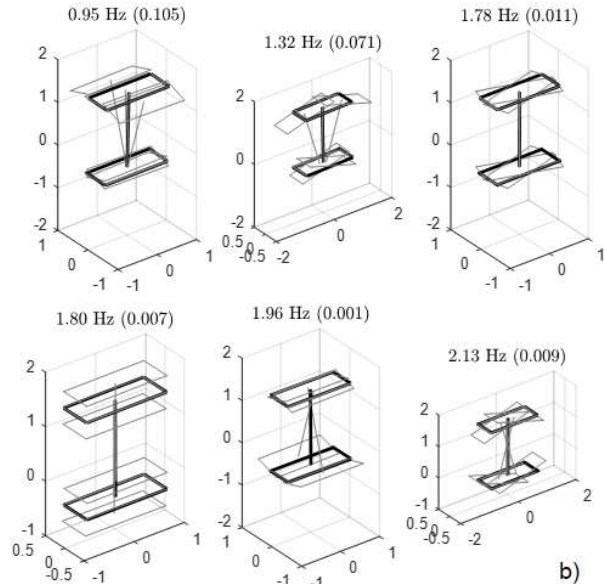


Fig. 18b. Modal shape with air springs height of 140 mm with stabilizers (the mode damping factor, due to the WRS, is indicated in brackets)

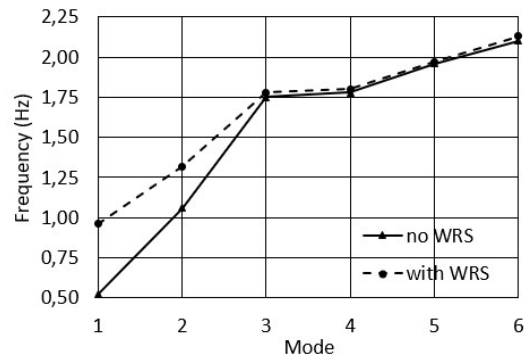


Fig. 19. Natural frequencies comparison

B. MR dampers influence

The presence of the MR-dampers further couples the system vibrating modes; the eigenvalue problem was solved for the minimum and the maximum MR damping value ($2 \cdot 10^3 \text{ Ns/m}$ and $15 \cdot 10^3 \text{ Ns/m}$); the correspondent frequencies and damping factors are reported in table III while the modal shapes, are shown in Figs. 20a and 20b, respectively. The modes are ordered considering their shape instead of the frequency to allow an easy comparison between the results obtained with the two damping values. It can be noted that for the maximum value of the MR damping, the second roll mode is overdamped.

TABLE III
FREQUENCIES AND DAMPING FACTORS FOR TWO DAMPING VALUES

2 kNs/m	f_j (Hz)	0.95	1.32	1.77	1.80	1.93	2.12
	ζ_j	0.107	0.103	0.134	0.081	0.181	0.055
15 kNs/m	f_j (Hz)	0.96	1.57	0.61	1.49		1.54
	ζ_j	0.112	0.191	0.940	0.559	>1	0.510
damping increase		+5%	+85%	+601%	+590%	>450%	+926%

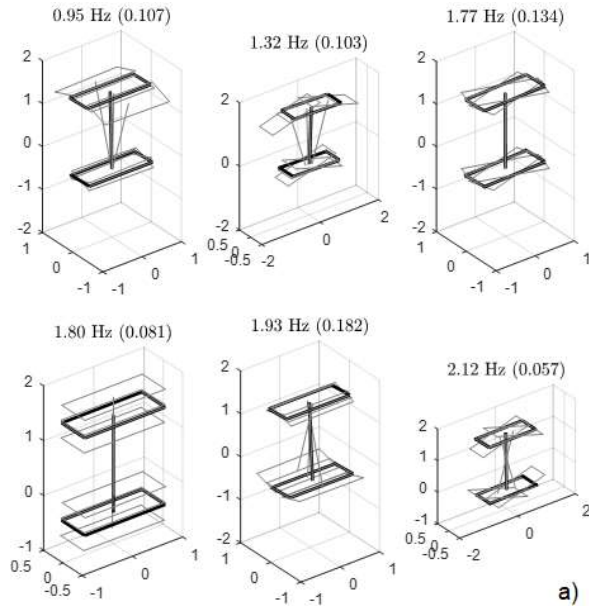


Fig. 20a. Rack modal shape for minimum damping

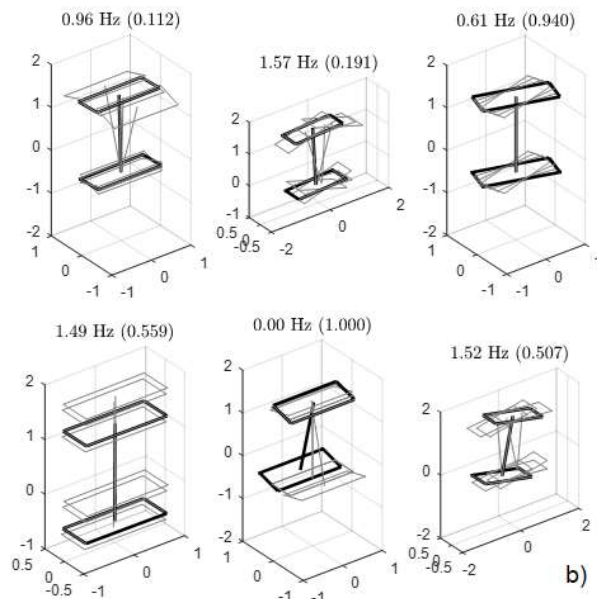


Fig. 20b. Rack modal shape for maximum damping

C. Acceleration transmissibility

The acceleration transmissibility of the suspension system was obtained by means of the frequency response of the system subjected to the base acceleration excitation along one of the x,y,z directions (Fig. 21). For each excitation direction,

the frequency response for the minimum and the maximum MR damping value, was defined.

The analysis highlights, one more time, that MR dampers can significantly improve the isolation of the system subjected to a base steady acceleration, except for an excitation at a frequency close to the first two natural modes (0.95 Hz and 1.32 Hz).

D. Air pressure influence

The air springs may exert the same vertical reaction at the height of 110 mm, but with a supply pressure of 2 bar instead of 3 bar. In this condition, the air spring axial stiffness increases while the transversal ones decrease:

$$k_z = 43 \text{ N/mm}; k_x = k_y = 17 \text{ N/mm.}$$

Therefore, a reduction in pressure in the air springs leads to an increase in the frequencies of the modes that mainly involve the axial stiffness of the springs (bounce roll, pitch) and a reduction of the remaining modes that mainly involve the shear stiffness (Table IV).

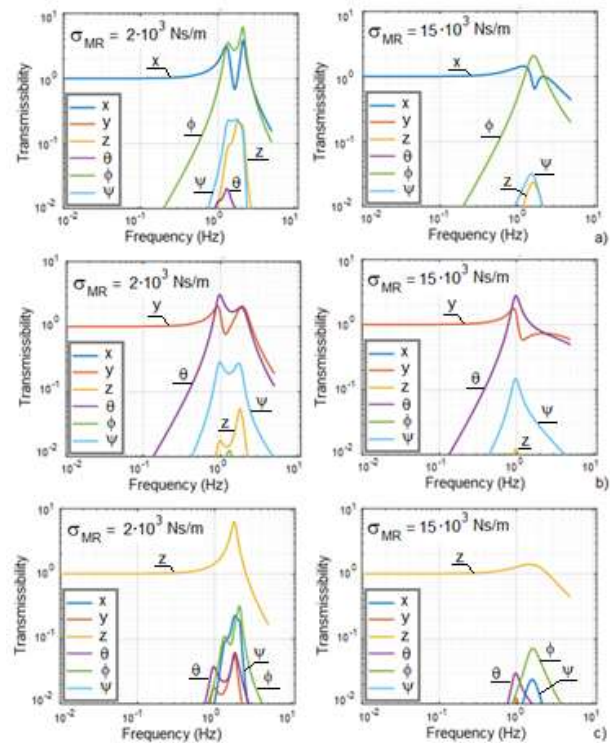


Fig. 21. Acceleration transmissibility along: a) X-axis, b) Y-axis; c) Z-axis

TABLE IV
FREQUENCIES AND DAMPING FACTORS

		I	II	III	IV	V	VI
		roll	pitch	yaw	bounce	2°roll	2°pitch
h=140	f_j (Hz)	0.95	1.32	1.78	1.80	1.96	2.13
mm	ζ_j	0.105	0.071	0.011	0.007	0.001	0.009
h=110	f_j (Hz)	1.04	1.38	1.58	2.35	1.76	2.19
mm	ζ_j	0.093	0.045	0.013	0.006	0.003	0.023
Δf (Hz)		+9.5%	+4.5%	-11%	+31%	-10%	+2.8%

D. Shock response

The rack shock response was evaluated applying a half-sine acceleration impulse to the base along the three reference

directions. The correspondent relative displacements and absolute acceleration time histories are plotted for different MR damping values.

The amplitude and the duration of the half-sine pulse has been chosen starting from an experimental acceleration measured on a truck floor during an off-road test. Selecting a section of the accelerogram containing the higher acceleration peak along the chosen direction, the corresponding shock response spectrum (SRS) has been evaluated; amplitude and duration of the half sine pulse has been chosen as its SRS overestimates the experimental one at lower frequencies (below 25 Hz).

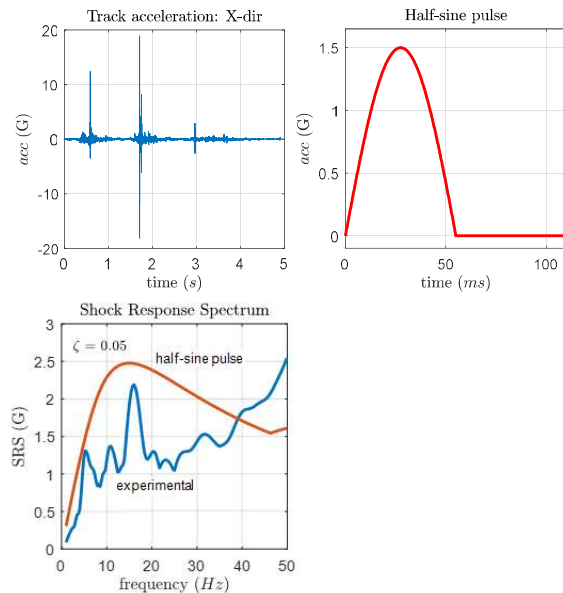


Fig. 22. Shock response: X-axis excitation

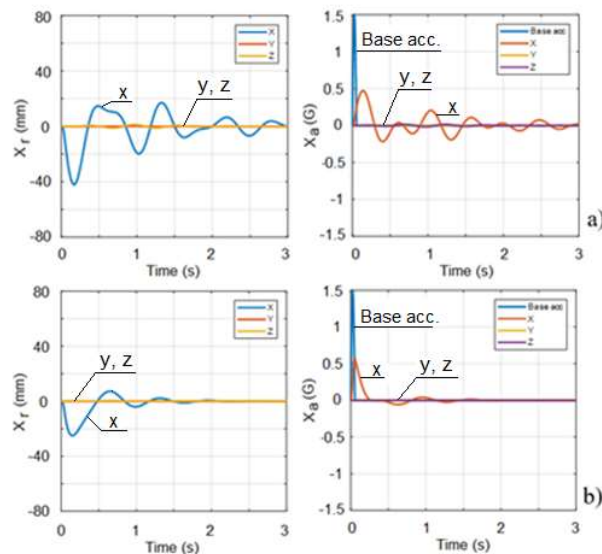


Fig. 23. Relative displacement and acceleration for: a) minimum damping level; b) maximum damping level

Fig. 22 reports the experimental truck floor acceleration, the half-sine pulse chosen for the shock simulation and the corresponding x directions SRS.

Adopting the SRS as input base acceleration, the integration of equation (12) allow to simulate the rack dynamic behaviour. Fig. 23 shows the obtained results, in case of horizontal X-excitation, in terms of displacement and acceleration diagrams, for the minimum and the maximum damping level.

It can be noted that the maximum relative displacement (see also Table V) is smaller than the stop bumper gap (50 mm) and that the maximum acceleration reaches acceptable values.

In this application it is significant to verify that the maximum relative displacement does not exceed the stop bumper gap as it would cause an impact between rack and cabin wall that, although mitigated by stop-bumpers, can lead to high acceleration values and damage to the equipment contained in the rack.

The results obtained for base excitation along X, Y, Z directions are summarized in Table V; for each direction, the amplitude and the duration of the half-sine pulse excitation is reported.

TABLE V
MAXIMUM DISPLACEMENT AND ACCELERATION FOR THE MINIMUM AND THE MAXIMUM DAMPING LEVEL

Pulse dir.	Ampl. (G)	Duration (ms)	Max. displ. (mm)	Max. acceleration (G)
x	1.5	55	42→25 (- 40 %)	0.47→0.58 (+ 23%)
y	2	50	39→25 (- 36 %)	0.43→0.74 (+ 72%)
z	4	50	40→23 (- 43 %)	0.53→0.60 (+ 13%)

V. THE TEST RIG

To experimentally investigate the proposed suspension system, a test rig was developed (Fig. 24). It is constituted by two steel frames made of tubular steel beams (60x5 mm):

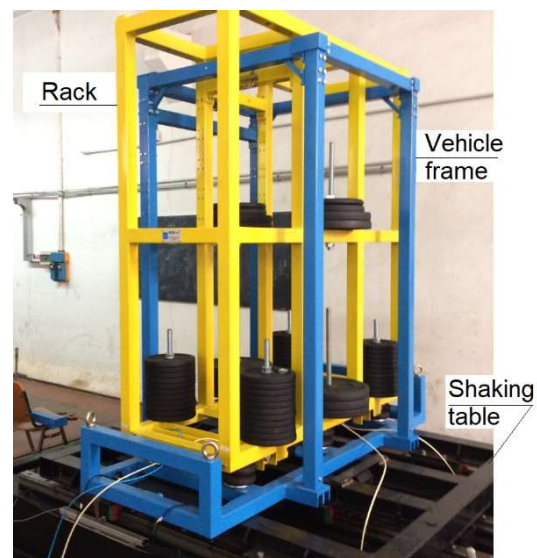


Fig. 24. The test rig: the rack (yellow coloured) is connected to the vehicle frame (cyan coloured) by means of the suspension system. The vehicle frame is fixed on the shaking table

- the first one (1596x600x1780 mm) represents a set of three racks; it is ballasted with metallic disks that simulate the presence of the devices contained in the rack;
- the second frame represents the *vehicle frame*; it comprises two elements, rigidly connected, simulating the floor and the wall of the vehicle cabin, respectively.

The two steel frames are connected, by means of the isolation system previously described (Figs. 25 and 26).

The air springs self-leveling system (Fig. 27) comprises a control unit for compressed air, an air compressor, a reservoir and six solenoid valves to independently adjust the pressure in each air spring.

The test rig was equipped with the following measuring instruments:

- two triaxial accelerometers (DSPM Mod. 4630), one fixed to the rack and the other one to the vehicle frame;
- four Draw-Wire Displacement Sensors (Micro-Epsilon Mod. WPS-250-MK30-P25), arranged in the vertices of the rack base to detect the vertical displacements with respect to the vehicle frame;
- two displacement potentiometric Transducer (Novotechnik TR 75) to detect the horizontal rack displacement;
- an IMU (LandMark MRM10) placed on the rack;
- a pressure sensor for each air spring (Parkers PTDVB0251B1C2, 0-25 Bar).

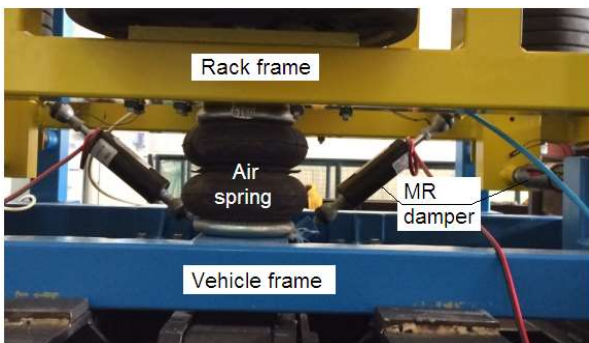


Fig. 25. Air springs and MR dampers placed under the rack



Fig. 26. Wire rope spring stabilizers

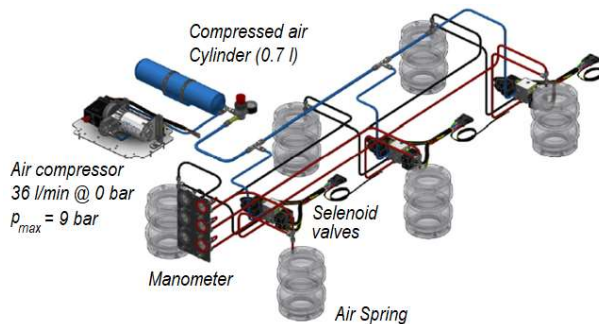


Fig. 27. Air springs pneumatic scheme

VI. THE EXPERIMENTAL TESTS

The preliminary tests were performed to check the functionality of the pneumatic system and of the measurement instrumentation.

Fig. 28 shows the signals of the four draw-wire displacement sensors in the rack self-levelling phase from the nominal height of 140 mm to that of 130 mm; a tolerance of ± 2 mm is allowed.

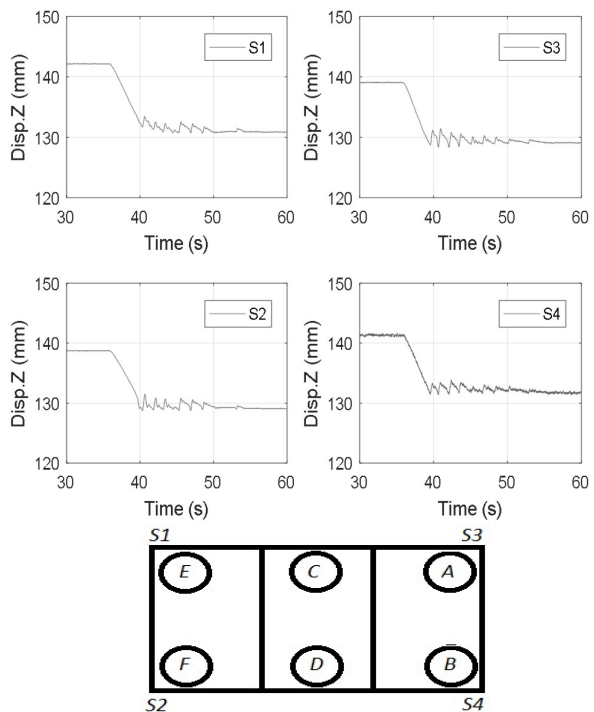


Fig. 28. Draw-wire sensors displacements in the self-levelling phase from the air spring height of 140 mm to that of 130 mm.

The rack will be tested on a 6 d.o.f. shaking table with the aim of defining the optimal heights of the air springs and the optimal inclination of the MR dampers.

In the following, the results of several preliminary tests are reported. These tests, conducted to evaluate the functionality of the isolation system components and of the instrumentation, were conducted with a reduced ballast (740 kg) and adopting a mono-axial shaking table [17] to excite the rack along its transversal direction.

During the tests the valves connecting the air springs to the compressed air reservoir were fully closed. Fig. 29 reports the response to a sweep frequency excitation characterized by a frequency variation of 0.02 Hz/s in the range 0÷5 Hz. The acceleration diagram, detected in transverse direction on the two frames, shows that, while the vehicle frame acceleration amplitude grows with a quadratic law, rack frame acceleration is almost constant. The correspondent vertical displacement of the rack lower corner S1, detected by the wire sensor, is amplified in correspondence of the roll and the transverse translation resonance (Fig. 30). The relative motion is amplified at about 65s and 130s and therefore, the two resonance frequencies arise at about 1.3 Hz (roll) and 2.6 Hz (transverse motion).

Finally, some tests were performed to test the MRDs; the shaking table was excited at a constant frequency, near a resonance condition and the MRDs were activated.

Fig. 31 shows the signal of the horizontal displacement sensors, positioned on the top and on the base of the rack. The test was performed at the frequency of 3.0 Hz, quite close to the natural frequency of the transverse motion. For the first 8 seconds the MRDs were not activated; the two signals are in phase and have almost the same amplitude; by activating the MRDs at the maximum damping value, there is an evident amplitude reduction of the bottom displacement (about 75%).

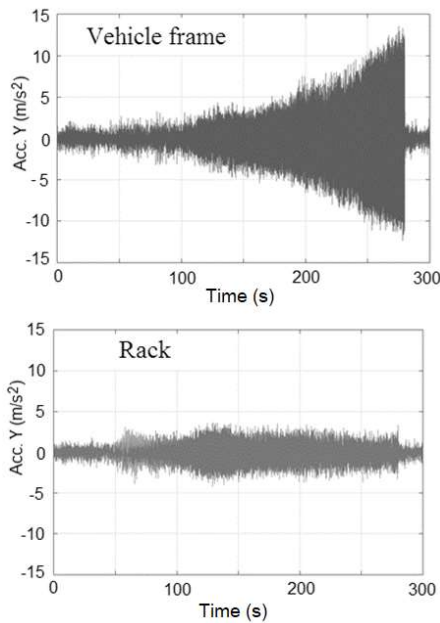


Fig. 29. Comparison between vehicle and rack frame horizontal acceleration for a frequency sweep excitation along the transverse direction

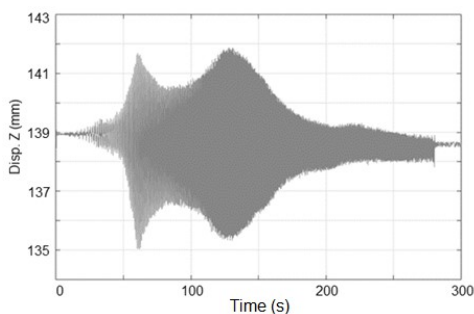


Fig. 30. Sweep test: rack vertical displacement

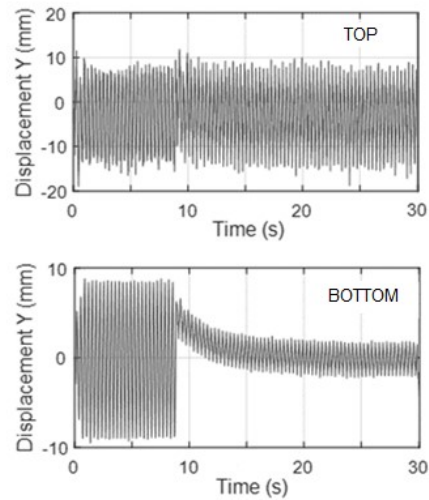


Fig. 31. Harmonic excitation at 3 Hz: horizontal rack response obtained by switching the damping value from minimum to maximum value

VII. CONCLUSIONS

An isolation system, for racks installed on board vehicles, has been proposed; it comprises air springs and magnetorheological dampers at the base and wire rope stabilizers on the top. Compared to the existing passive systems, constituted only by wire rope springs, it is certainly more complex, as it requires the use of a pneumatic control unit and a self-leveling control system. However, in case of replacement of the devices, it allows the rack to maintain the correct attitude and the same efficiency of isolation from vibrations.

The rack natural frequencies, depending on the axial and transverse air springs stiffness, may be changed adjusting the air pressure; moreover, the rack dynamics can be controlled adjusting the damping level with the aim of finding the best tradeoff to achieve low accelerations compatibly with the maximum values of the possible displacements.

The first experimental tests, although performed on a mono-axial shaking-table and with a lower ballast, have shown the possibility to develop a control system that can improve the efficiency of the insulation system.

ACKNOWLEDGMENT

The authors are grateful to Giuseppe Iovino, Gennaro Stingo and Pierpaolo Placenza (ESI Italia srl) for their collaboration during the setup construction and the execution of laboratory tests.

AUTHOR CONTRIBUTIONS:

All the authors participated in the conceptualization, investigation and writing phases.

REFERENCES

- [1] T.D. Gillespie, *Fundamentals of vehicle dynamics*, SAE Warrendale, PA, 1992.
- [2] G. Zepeng, N. Jinruia, L. Liana, X. Xiaolina, Research on air suspension control system based on fuzzy control”, *Energy Procedia* n.105, pp. 2653–2659, 2017.
- [3] D.H. Wang, W.H. Liao “Magnetorheological fluid dampers: A review of parametric modeling”, *Smart Materials and Structures*, vol. 20, n.2, 2011.

- [4] R. Brancati, G. Di Massa, S. Pagano, S. Santini, "A magneto-rheological elastomer vibration isolator for lightweight structures" *Meccanica*, vol.1-2, 2019.
- [5] G. Quaglia, M. Sorli, "Analysis of vehicular air suspensions", Proc. of Fourth JHPS International Symposium on Fluid Power, pp. 389-384, Tokyo, 1996.
- [6] C. M. Harris, A.G. Piersol, *Harris' shock and vibration handbook*, Fifth Edition, McGraw-Hill, 2002.
- [7] G. Di Massa, S. Pagano, S. Strano, "Stability Analysis of Air Springs Subjected to Lateral Loads" Proc. of the World Congress on Engineering, 2017,
- [8] W. Kordonsky, "Magnetorheological effect as a base of new devices and technologies" *Journal Magn. Magn. Mater.*, vol. 122, pp.395-398, 1993.
- [9] Franklin Y.C., Hongping J., Kangyu L., *Smart Structures: Innovative Systems for Seismic Response Control*, CRC Press, 2008.
- [10] F. Tu, Q. Yang, C. He, L. Wang, "Experimental Study and Design on Automobile Suspension Made of Magneto-Rheological Damper", Int. Conf. on Future Energy, Environment and Materials, pp.417-425, 2012.
- [11] T. Feng, T. Shun-Hsu, W. Jeffrey, "An Investigation on Mathematical Models of Wire Rope Isolators" The 30th National Conference on Theoretical and Applied Mechanics, DYU, Changhwa, Taiwan, R.O.C. Dec.15-16, 2006.
- [12] P.S. Balaji, L. Moussa, M.E. Rahman, L.H. Ho, "An analytical study on the static vertical stiffness of wire rope isolators", *Journal of Mechanical Science and Technology* vol.30, n.1, pp. 287-295, 2016.
- [13] R.R. Gerges, B.J. Vickery, "Design of tuned mass dampers incorporating wire rope springs: Part I: Dynamic representation of wire rope springs" - *Engineering Structures* n.27, pp.653-661, 2005.
- [14] G. Kelly, *Mechanical Vibrations. Theory and Applications*, Cengage Learning, 2012.
- [15] K. Kecik, A. Mitura, D. Sado, J. Warminski "Magnetorheological damping and semi-active control of an autoparametric vibration absorber", *Meccanica*, vol.49, n.8, pp.1887-1900, 2014.
- [16] G. Di Massa S. Pagano, S. Strano, "Cabinet and Shelter Vibration Isolation: Numerical and Experimental Investigation", *Engineering Letters*, vol.22, n.4, pp.149-157, 2014.
- [17] S. Pagano, M. Russo, S. Strano S., M. Terzo, "Seismic isolator test rig control using high-fidelity non-linear dynamic system modeling", *Meccanica*, vol. 49, n.1, pp.169-179, 2014.